

# Microbial Removal of Ionic Mercury in a Three-Phase Fluidized Bed Reactor

W. -D. DECKWER,\*† F. U. BECKER,‡  
S. LEDAKOWICZ,§ AND  
I. WAGNER-DÖBLER†

GBF - Gesellschaft für Biotechnologische Forschung mbH,  
Braunschweig, Germany, Degussa AG, Frankfurt, Germany,  
and Technical University Lodz, Poland

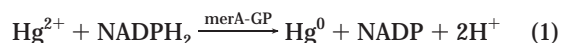
The reductive biotransformation of mercuric ions to elemental mercury was studied by applying a model system with a genetically engineered *Pseudomonas putida* strain in a lab scale three-phase fluidized bed (TPFB). The aim was to demonstrate the suitability of the TPFB to demercurize effluent streams containing up to 10 mg Hg<sup>2+</sup> dm<sup>-3</sup>. The TPFB is used, first, to carry out the biotransformation on the alginate immobilized biocatalyst and, second, to remove the produced Hg<sup>0</sup> by volatilization into the gas phase followed by its recovery through fast oxidative absorption. Targeted experiments with the immobilized biocatalyst were designed and carried out to determine mercury adsorption data on the biomass and all relevant mass transport rates at conditions prevailing in the TPFB. The evaluation of the performance data in the TPFB revealed almost complete reaction control and hence negligibility of mass transfer resistances. This simplifies the scale-up of larger TPFB reactors for mercury removal as it can be based on the known kinetics alone. The measured biotransformation capacities in the TPFB are similar to those reported for the fixed bed technology which has already proven its applicability at an industrial scale in long time runs. However, the TPFB offers some advantages over the fixed bed and could therefore possibly be a favorable, reliable, and less costly alternative to the existing technology.

## 1. Introduction

**1.1. Mercury Applications.** Mercury (Hg) and its compounds are all toxic. Despite their toxic properties, they are widespread in nature and have found numerous industrial and medical applications. Examples are fungicides, disinfectants, dental products, catalysts, ammunition igniters, protection colors, etc. The formation of amalgams is a specific property being used in gold leaching and the chlor-alkali electrolysis process. Though new alternatives have been developed the amalgam route is still the base of about 40% of the worldwide chlorine production (roughly 26 Mio t in 2000). Each electrolysis cell producing 2000–4000 t Cl<sub>2</sub>/a requires about 1 t of Hg per a. Although many improvements and sophisticated recycle streams were realized in the industrial

amalgam process, it is not possible to avoid the release of some Hg containing wastewater (1). The limiting discharge value for the wastewater is 50 µg/dm<sup>-3</sup> and is usually achieved by ionic exchange resins. Another considerable emission of Hg into the environment is caused by combusters and power stations (2). The particular problem with mercury in the environment is, first, its potential for remobilization even from low soluble forms through microbial generation of methylmercury and, second, its ability to accumulate in nutrition chains (3).

**1.2. Microbial Mercury Resistance.** However, mercury is not only widely distributed by anthropogenic activities but above all as a result of geochemical and biological phenomena. They all contribute to the global mercury recycle with fluxes of several tons of Hg per a (3). It is therefore understood that in the course of evolution effective microbial resistances could develop. The microbial resistance mechanism is the transformation of Hg(II) compounds in metallic mercury (Hg<sup>0</sup>) which is obviously less toxic for microorganisms. The reaction commences stoichiometrically under consumption of biochemical reduction equivalents (NADPH<sub>2</sub>) in the microbial cell



The biotransformation is catalyzed by the enzyme mercury reductase, the product of the merA gene. More details of the resistance mechanism and the structure and function of the involved genes (mer operon) can be found in the literature (4, 5).

**1.3. Fixed Bed Process for Mercury Removal.** Using mercury resistant bacteria, a fixed bed reactor technology has been developed for Hg removal from wastewater of chlor-alkali electrolysis plants (6, 7). The fixed bed reactor (1 m<sup>3</sup> volume) was used to clean the wastewater of two European chlorine factories (about 50.000 m<sup>3</sup> over a period of 2 years). Though the fixed bed offers various advantages (simplicity, robustness, cost-effectiveness), its major drawback is the accumulation of Hg in the bed which, on the one side, may lead to clogging and disturbances of the uniform flow through the particle bed, and, on the other side, yields a Hg<sup>0</sup> outlet concentration of 20–60 µg dm<sup>-3</sup> due to the physical solubility of mercury. In addition, colloidal mercury eventually bound to microbial flocs is found in the effluent stream. This effects make it difficult to maintain the limiting discharge value (50 µg dm<sup>-3</sup>) with the bioreactor alone. Another weakness of the fixed bed operation is that accumulated Hg cannot be withdrawn out of the reactor. Thus, after a period of several months on stream the particle bed with the immobilized biocatalyst and the generated metallic Hg must be substituted by a new bed with either a new or regenerated filling of support particles, respectively.

**1.4. Goal of Present Work.** In view of these problems and the difficulties encountered with the long-term fixed bed operation it was thought that three-phase fluidization could be an advantageous alternate technology (8, 9). In the TPFB the biocatalyst is immobilized on the solid matrix and fluidized by the circulation flow induced by rising bubbles and thus providing for a uniform reaction rate in a gradientless reactor. Furthermore, the produced Hg<sup>0</sup> can be volatilized into the gas bubbles due to its high vapor pressure. Thus, the product is removed from the reaction phase and captured from the gas phase by absorption in an oxidative liquid phase. The goal of this study was (1) to demonstrate the feasibility of the TPFB for the demercurization of aqueous solutions, (2) to find out the rate-limiting steps, and (3) to

\* Corresponding author phone: +49 531 6181-100; fax: +49 531 6181-175; e-mail: WDD@GBF.de. Mailing address: GBF/TU-BCE, Mascheroder Weg 1, D-38124 Braunschweig, Germany.

† GBF - Gesellschaft für Biotechnologische Forschung mbH.

‡ Degussa AG.

§ Technical University Lodz.

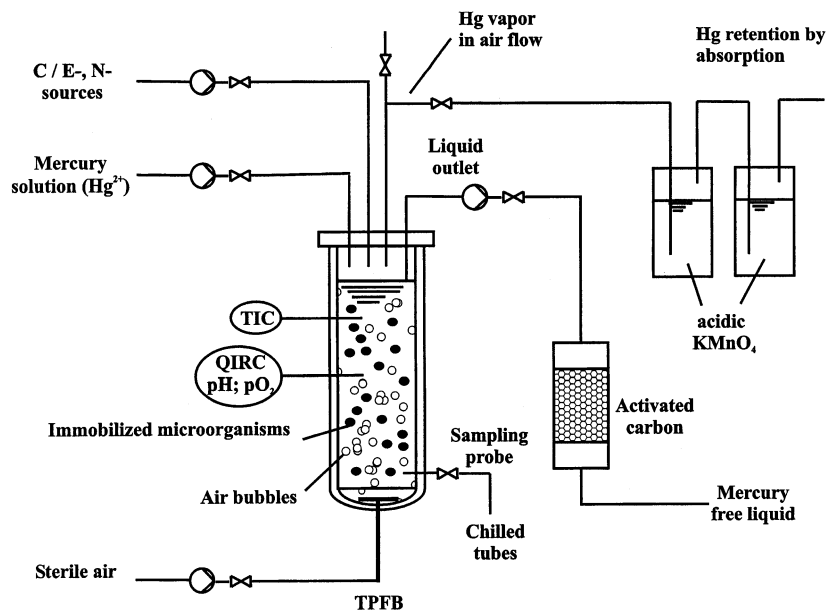


FIGURE 1. Experimental setup of the TPFB reactor for microbial mercury transformation and its off-transport via the gas phase.

compare the performance of the fluidized bed system with the fixed bed reactor technology.

## 2. Materials and Methods

The microorganism used as a biocatalyst in this study was *Pseudomonas putida* KT2442::mer73 with a minitransposon containing the mer TPAB operon (10). This genetically engineered microorganism belongs to the lowest risk class and is not only able to reduce ionic mercury at higher concentrations and rates but also has a wider substrate spectrum (for instance, organomercurials). The organism was stored as a glycerol conserve at  $-20^{\circ}\text{C}$ . Cultivation was done with a standard medium with acetate or glucose as the carbon and energy source.

The *P. putida* strain selected was immobilized in alginate. Preparation of the hydrogel beads was done from the aqueous solution of the alginate with the suspended biocatalyst. The suspension droplets fell into a solution of  $\text{CaCl}_2$  (2 wt %). By variation of the needle diameter used for drop formation and the operation conditions (concentrations, pressure, and drop blow-off flow), the diameter of the alginate beads could be altered from 0.8 to 3 mm. The details of the gel encapsulation techniques are reported elsewhere. The biomass concentration in the alginate particles is given in % w/w (g dry biomass  $\times$  100/g alginate).

The immobilized microorganisms were used in a  $1.5\text{ dm}^3$  three phase fluidized bed (TPFB) reactor (Bioengineering AG, Switzerland) with a working volume of  $1.0\text{ dm}^3$ . The reactor was controlled at  $30^{\circ}\text{C}$  and pH 7 and is schematically shown in Figure 1.  $\text{Hg(II)}$  chloride solutions (with concentrations  $\leq 10\text{ mg dm}^{-3}$   $\text{Hg(II)}$ ) containing additionally nutrients ( $5\text{ g dm}^{-3}$  glucose,  $0.1\text{ g dm}^{-3}$  yeast extract, and mineral medium M63) was fed to the TPFB with immobilized *P. putida* (about  $1.2\text{ g dm}^{-3}$ ). The liquid effluent contains only little  $\text{Hg}$  ( $\leq 150\text{ }\mu\text{g dm}^{-3}$ ) and passes an activated carbon filter which removes all  $\text{Hg}$  by adsorption. Over 95% of the ionic mercury fed to the bed is taken up by the gas phase (air flow rate:  $2\text{--}5\text{ cm s}^{-1}$ ) after its reduction to volatile  $\text{Hg}^0$ . The airflow also guaranteed a sufficient oxygen supply for maintenance and possibly growth of the life biocatalyst which also has to provide the reduced cofactor ( $\text{NADPH}_2$ , eq 1). The  $\text{pO}_2$  in the liquid phase was measured by a polarographic probe (Ingold, Switzerland) and always found above 80% air saturation. The outlet gas was fed to the  $\text{Hg}$  vapor absorption system which consisted of a stirred cell and one or several washing bottles filled with  $\text{KMnO}_4/\text{H}_2\text{SO}_4$  solution (12) followed by a

sulfurated carbon filter (not shown). The mercury content in the inlet and outlet liquid flow and in the gas trap device was measured periodically (usually every hour) by using atomic absorption (Perkin-Elmer M 2100) with cold vapor and hydride formation techniques. The TPFB could be operated in batch, fed batch, and continuous mode. Some runs were also done with two reactors in a series (continuous mode). No special precautions were taken to guarantee monoseptic operation. Only the preparation of the immobilized biocatalyst was carried out in a laminar flow bench.

The experimental techniques to determine equilibrium data and transport parameters are briefly mentioned when dealt with in part 3 of this paper. They are usually well-known and are reported elsewhere in more detail (11). The nonresistant parent strain *P. putida* KT 2442 which does not have the mer operon and, hence, cannot carry out the mercury transformation (eq 1) was used in these experiments.

## 3. Transport Phenomena Involved in TPFB Operation

**3.1. Course of Biotransformation.** The biotransformation of ionic  $\text{Hg}$  to the metallic form takes place in the cell interior of the immobilized microorganisms. The ionic mercury enters the reactor with the wastewater which also contains some nutrients (such as BOD, acetate, or glucose). The reduced  $\text{Hg}$  leaves the TPFB via the gas phase as volatile metal. The overall process is schematically shown in Figure 2 which also points out to the various transport phenomena.

The following individual steps can be identified: (a) liquid/solid mass transfer of  $\text{Hg}^{2+}$  from the bulk liquid to the particle surface characterized by  $k_{SAS}$ , (b) simultaneous effective diffusion with a biological reaction inside the immobilized biocatalyst ( $D_{\text{eff}}$  of  $\text{Hg}^{2+}$ , kinetic data), (c) effective diffusion of generated elemental  $\text{Hg}^0$  in the immobilizate ( $D_{\text{eff}}$  of  $\text{Hg}^0$ ), (d) liquid–solid mass transfer of  $\text{Hg}^0$  through the liquid film around the biocatalyst particle ( $k_{SAS}$  of  $\text{Hg}^0$ ), and (e) gas–liquid mass transfer of  $\text{Hg}^0$  ( $k_{L,a}$  of  $\text{Hg}^0$ ).

Due to the small size of  $\text{Hg}^0$  as compared to the hydrated  $\text{Hg}^{2+}$  and its uncharged state it is assumed that steps (c) and (d) are fast and hence negligible in comparison to steps (a), (b), and possibly (e). Furthermore, the transport of the energetic carbon source to the biocatalyst is not considered as a limiting factor since the reducing equivalents are in excess as a result of nutrient supply. For estimation of the mass fluxes, one does not only require the knowledge of the

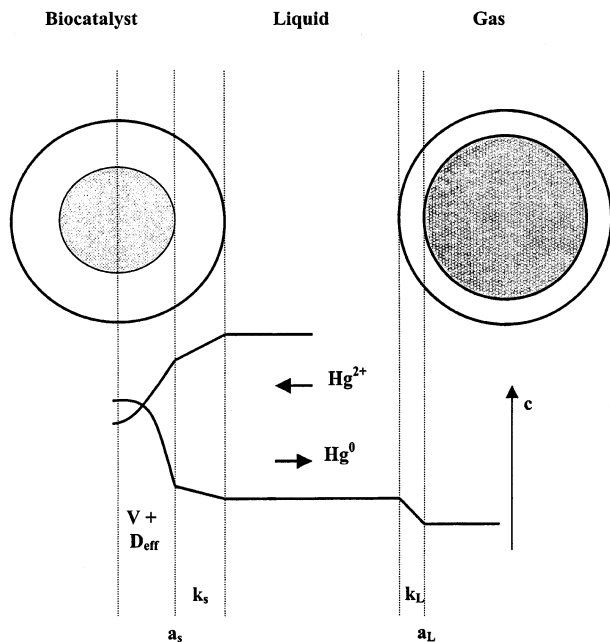


FIGURE 2. Course of mercury concentration (in ionic and metallic form) in the various phases of the TPFB.

kinetic data and the transport coefficients but also some equilibrium data.

**3.2. Physical Equilibria.** The solubility of  $\text{Hg}^0$  in water ( $c^0$ ) was experimentally determined in the temperature range of 10–46 °C. Their own measurements were correlated with literature data (28–120 °C). Thus the subsequent relation was obtained (11)

$$\ln c^0 = 18.2 - 4427/T \quad (2)$$

Here  $c^0$  is in  $\mu\text{g dm}^{-3}$  and  $T$  is in K. The equilibrium distribution of a gas component ( $\text{Hg}^0$ ) between the liquid and gas phase is usually described by Henry's law

$$\text{He} = p/c_1^* \quad (3)$$

where  $p$  is in  $\text{Pa}c_1^*$  in  $\mu\text{g dm}^{-3}$  and  $\text{He}$  is in  $\text{Pa, dm}^3 \mu\text{g}^{-1}$ . The Henry constant for water as a liquid phase was measured carefully by assuming ideal gas behavior for  $\text{Hg}^0$ , and correlation with the available literature data (2–46°) yielded the following correlation (regression coefficient: 0.97)

$$\ln \text{He} = 8.54 - 4150/T \quad (4)$$

For the estimation of the effective diffusivities of  $\text{Hg}^{2+}$  in the immobilized biocatalyst by using pore diffusion models knowledge of the adsorption of  $\text{Hg}^{2+}$  mercury on the inert alginate particles as well as on those loaded with the biomass is required. Therefore, adsorption isotherms for  $\text{Hg}^{2+}$  were measured at 30 °C and pH 7. The alginate particles contained roughly 5, 10, and 20% (w/w) of biomass which was the wild strain *Pseudomonas putida* KT2442. This microbe does not have the mercury resistant genes and, hence, does not reduce  $\text{Hg}^{2+}$ .

The adsorption data can be well described by the Langmuir isotherm

$$Q/Q_{\text{max}} = K_A c_1 / (1 + K_A c_1) \quad (5)$$

If the loadings  $Q$  were referred to as biomass (free or immobilized)  $Q_{\text{max}}$  is about 210 mg of  $\text{Hg}^{2+}$  per g of biomass, while the affinity constants  $K_A$  are 0.8, 0.3, 0.17, and 0.08  $\text{dm}^3 \text{mg}^{-1}$  for free biomass and alginate particles with 5, 10, and

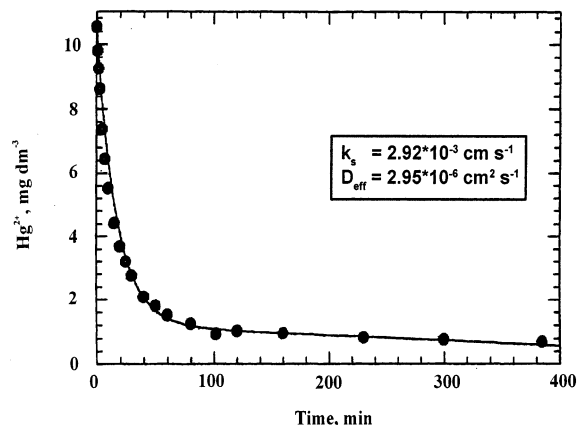


FIGURE 3. Time course of mercury concentration (points) and model prediction (14) with optimization of  $k_s$  and  $D_{\text{eff}}$ . Alginate particles with  $d_p = 1.24$  mm and 5% (w/w) biomass *P. putida* KT2442,  $u_G = 0.25$  cm/s.

20% w/w biomass, respectively. Alginate particles without biomass do not adsorb any ionic mercury.

### 3.3. Physical Transport Parameter.

**3.3.1. Liquid–Solid Mass Transfer Coefficient.** The mass transfer of ionic mercury from the bulk liquid to the particle surface is characterized by  $k_s a_s$ , and the mass transfer rate is given by

$$\frac{dc_1}{dt} = k_s a_s (c_1 - c_s) \quad (6)$$

By exposing swollen particles with immobilized nonresistant biomass (*P. putida* KT2442) into a solution of  $\text{Hg}^{2+}$ , the decline of  $c_1$  under the conditions existing in the TPFB can easily be measured. With consideration of the initial conditions ( $c_1 = c_1^0$  and  $c_s = 0$  for  $t = 0$ ) the slope ( $dc_1/dt$ ) of the curve at  $t = 0$  and hence  $k_s a_s$  can be determined.

The  $k_s a_s$  data measured in the TPFB show the following features: the gas velocity has no significant effect on  $k_s a_s$  provided  $u_G \geq 1$   $\text{cm s}^{-1}$ , the  $k_s a_s$  data do not depend on the biomass fraction of the particles, and there is an influence of the immobilization matrix and  $d_p$  even if the effect of  $d_p$  on  $a_s$  is properly accounted for ( $a_s = 6\epsilon_p/d_p$ ).

Typical  $k_s$  values are in the range of  $2-4 \times 10^{-3}$   $\text{cm s}^{-1}$  and about 20–30 times larger than those calculated from the minimum limiting value:  $\text{Sh} = 2$ . This increase is due to the system's turbulence caused by the rising bubbles in the TPFB. Further details on  $k_s a_s$  can be found by Becker (11).

**3.3.2. Intraparticle Diffusivity.** To further evaluate the Hg transformation process made it necessary to study the rate of adsorption, i.e., the rate of ionic mercury uptake by intraparticle diffusion within the immobilize (*P. putida* KT2442). A typical example of the time course of  $\text{Hg}^{2+}$  in the presence of alginate beads (about 2000 beads of 1.24 mm diameter) with 5% (w/w) inert biomass (KT2442) fluidized in the TPFB with  $u_G = 0.25$   $\text{cm s}^{-1}$  is shown in Figure 3. The data were evaluated with a closed solution of a simple model proposed by Crank (13) and a more sophisticated model (14) which among others accounts for external mass transfer around the particle. By using the Marquardt optimization procedure both models deliver effective diffusivities which differ only little. The optimized values of  $D_{\text{eff}}$  are independent of the gas velocity used in the TPFB and showed little dependency on the particle diameter in the range of 1–2.8 mm. The model description of the Hg uptake curves (Figure 3) show little sensitivity for  $k_s$ . The model of Arve and Liapis (14) gives  $k_s$ -data which are in agreement with the independently measured  $k_s$  (3.3.1). However, a remarkable dependency of  $D_{\text{eff}}$  on the encapsulated biomass was observed. Surprisingly, the effective diffusivity increased with

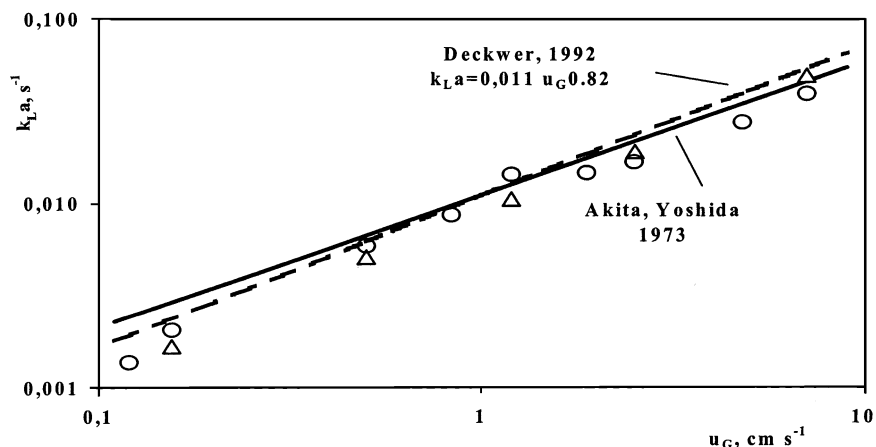


FIGURE 4. Volumetric liquid side mass transfer coefficients ( $k_L a$ ) for  $Hg^0$  desorption from water as function of gas velocity.

TABLE 1. Effective Diffusivities in Alginate

biomass content, % w/w	mean particle diameter, mm	$D_{eff} \times 10^6,$ $cm^2 s^{-1}$
5	2.2	2.1
9	2.5	4.5
17	2.5	6.3
	2.6	9.7

the rising biomass concentration in the gel beads (Table 1). This finding is in contrast to observations reported in the literature where the diffusivity of small molecules (phenol, lactate,  $O_2$ ) decreases with an increasing biomass imbedded in the gel particles (15). The reason for this unexpected behavior is that the measured “adsorption isotherms” do not really refer to physical equilibria as the adsorption phenomena observed are largely irreversible. Indeed, the mercury ions are bound to the cell wall by ionic forces, chelating effects, etc. Hence, even in the case of the nontransforming biomass adsorption is accompanied by an irreversible reaction chemisorption which leads to an apparent enhancement of the intraparticle diffusion in the models applied. This specific phenomenon does not disturb the intended estimations as under real process conditions with the immobilized biocatalyst the  $Hg^{2+}$  is reduced to  $Hg^0$ .

**3.3.3. Gas-Liquid Mass Transfer.** In this study of  $Hg$  transformation in a TPFB, the produced elementary  $Hg$  is removed from the reaction locus in the cell interior to the gas phase by desorption. While it is anticipated that diffusive transport and solid-liquid mass transfer of  $Hg^0$  is less important than for  $Hg^{2+}$  (hydrated) and probably negligible, no information is available about the gas-liquid mass transfer of a volatile metal such as  $Hg^0$ . Therefore, the desorption of  $Hg^0$  was investigated in the batch mode. To this end  $Hg^0$  was dissolved in water in a stirred vessel. One  $dm^3$  of the solution (with  $14.5 \mu g dm^{-3} Hg^0$ ) was transferred to a TPFB of 5 cm diameter, and the time course of dissolved  $Hg^0$  was measured with and without the presence of suspended alginate particles at various gas velocities. The  $k_L a$  data were evaluated from the desorption curves by

$$\frac{dc_1}{dt} = k_L a (c_1 - c_1^*) \quad (7)$$

with  $c_1^* = p/He$ . With the initial condition at  $t = 0$ :  $c_1 = c_1^0$  one obtains

$$c_1(t) = p/He + (c_1^0 - p/He) \exp(-k_L a t) \quad (8)$$

This equation was used to evaluate  $k_L a$  from the experimental data by Marquardt’s algorithm.

The desorption rate (proportional to  $k_L a$ ) increases with rising gas velocity. The presence of alginate particles did not significantly vary the mass transfer behavior as could be expected from the gas hold-up measurement which showed no effect of the suspended solid ( $\leq 40 g dm^{-3}$ ). The  $k_L a$  data calculated from the desorption curves are shown in dependence of the gas velocity in Figure 4. The measured data are in reasonable agreement with the correlation of Akita and Yoshida (16) which can be reduced to

$$k_L a \propto d_r^{0.17} u_G^{0.7} \quad (9)$$

where  $d_r$  is the reactor diameter and  $u_G$  is the gas velocity (17).

**3.4. Rate of Biotransformation.** The kinetic of the biotransformation, eq 1, was studied with freely suspended cells of the resistant strain *P. putida* KT2442::mer73, hence any diffusional limitations were avoided. A special experimental set up and various assay conditions were applied to measure the  $Hg^{2+}$  reduction rate under variation of the concentrations of ionic mercury and the reducing cofactor  $NADPH_2$  (11). To obtain information about the mercury transport through the cell wall rates were also measured with both intact and permeabilized cells.

The rate data evaluation led to an ordered bi-bi-mechanism involving the formation of tertiary complexes with both substrates as inhibitors. While the cofactor acts competitively, the ionic mercury is an uncompetitive inhibitor. The formulation of all the intracellular enzymatic reaction steps can be advantageously done with the King-Altman method (18). The sophisticated kinetic expression can be drastically simplified by introducing a constant  $NADPH_2$  concentration (either as result of the stationary equilibrium state or present in excess). Thus the well-known Haldane rate equation for noncompetitive inhibition is obtained (18). Under conditions prevailing at the reactor operation the measured data are best described by an extended Haldane expression (19)

$$v = \frac{v_{max}}{1 + K_S/c + (c/K_I)^2} \quad (10)$$

As shown in Figure 5 the experimental data are excellently described with the following optimized parameter values

$$v_{max} = 38.64 \mu g \min^{-1} mg^{-1} \quad (\text{referred to mass of cell protein})$$

$$K_S = 4.52 mg dm^{-3}$$

$$K_I = 0.62 mg dm^{-3}$$

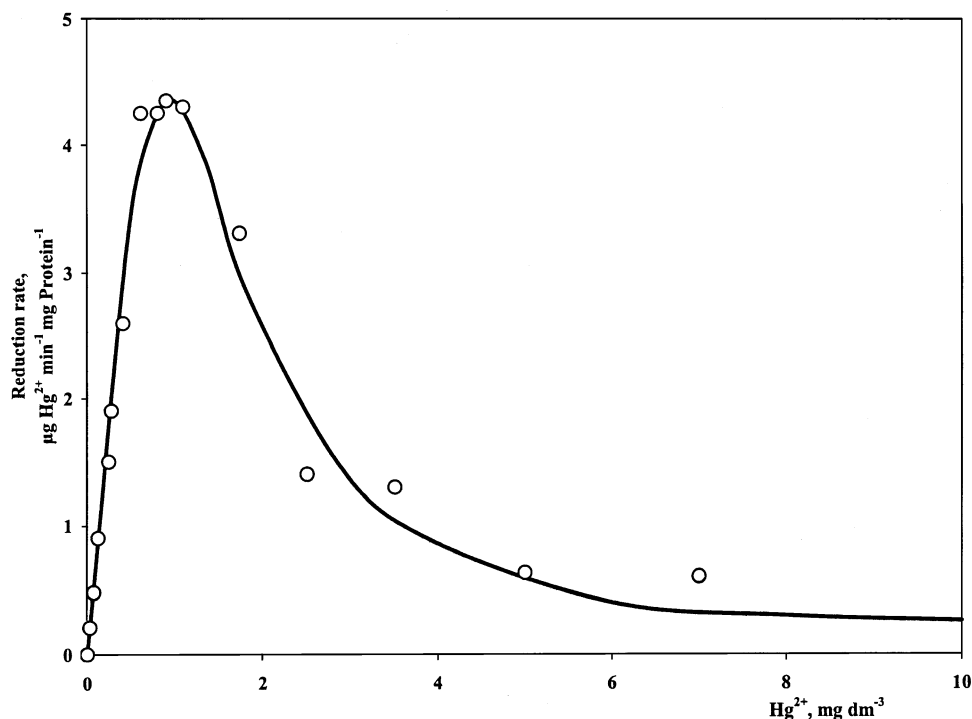


FIGURE 5. Initial rates of ionic mercury reduction by *Ps. putida* (KT2442::mer73). The experimental data are well described by the Haldane expression for substrate inhibition, eq 10.

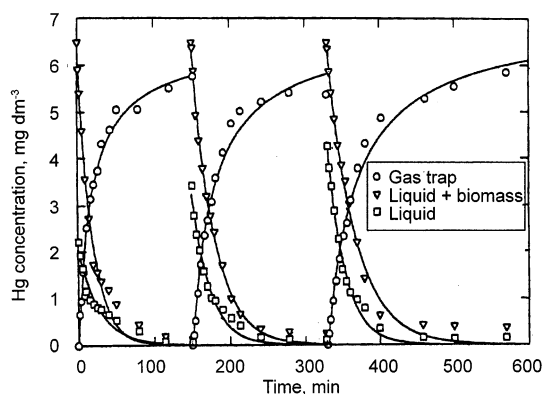


FIGURE 6. Biotransformation of  $\text{Hg}^{2+}$  by nonimmobilized cells of *Ps. putida* KT2442::mer73 in three repeated batch runs in TPF.

The optimum rate is about  $4.4 \mu\text{g min}^{-1} \text{mg}^{-1}$  for a  $\text{Hg}^{2+}$  concentration in the range of  $0.5\text{--}1.2 \text{ mg dm}^{-3}$ . At low concentrations, say  $< 0.5 \text{ mg dm}^{-3}$ , the above rate expression reduces to first-order behavior

$$v = (v_{\max}/K_S)c \quad (11)$$

with an error  $< 15\%$ . The rates measured with permeabilized cells also indicate that the microbial biotransformation is predominantly governed by the catalytic reduction and not by cellular transport phenomena.

#### 4. Reactor Performance

At first the biotransformation with *Ps. putida* KT2442::mer73 was investigated batchwise in the TPF. The microorganisms were applied either in free suspension or immobilized in alginate. All runs were performed at a gas velocity of  $4.9 \text{ cm s}^{-1}$ , and the conditions are given in section 2. Figure 6 shows the experimental data of a batch run with nonimmobilized biomass. The run was started by injection of  $\text{HgCl}_2$  solution, and the mercury concentration of the aerated biomass suspension and the biomass free liquid phase (supernatant

after centrifugation) are given as a function of time. Also given is the overall amount of elemental mercury (per volume of suspension phase) removed from the reaction phase by mass transfer into the gas phase. The removed mercury was calculated from the mercury collected in the gas-phase traps. As indicated by both the steep decrease of the Hg in the suspension phase and its corresponding increase in the gas phase, the biotransformation immediately starts (after  $\text{HgCl}_2$  addition). Noticeable is particularly the distinct concentration difference between mercury in the suspension and the liquid phase. This difference must be attributed to adsorption of  $\text{Hg}^{2+}$  (and probably also elemental  $\text{Hg}^0$ ) on the biomass. Indeed, one can estimate from the adsorption isotherms (3.2) that the difference in the concentrations can be in the range of several  $\text{mg dm}^{-3}$  as observed in Figure 6. It is also discerned from Figure 6, that the suspension and liquid-phase concentrations of mercury do not reduce to zero. Even after longer aeration the mercury which is supposed to be in the unloaded elemental state is not removed via the gas phase. Therefore, it is anticipated that a small amount of Hg is bound to the biomass and additionally stable  $\text{Hg}^0$  complexes in low concentrations may be formed with complexing components produced from the medium and proteins generated by intact biomass or cell lysis. The existence of stable Hg complexes and the impossibility to volatilize Hg from such solutions was shown by independent measurements with culture supernatants. Such a behavior can also be expected from literature reports (20).

Mercury accumulation and biomass deactivation are detrimental effects for the development of a robust mercury remediation process. Therefore, the number of repeated batch runs was increased using again a nonimmobilized biomass. Table 2 summarizes the results of 9-fold repeated batch runs (series B) including an overnight resting phase. Again a small increase in the residual mercury concentrations is observed (not shown). However, surprisingly the overall specific mercury conversion rate  $R_0$  calculated from  $\text{Hg}^0$  accumulation in the gas traps remained constant after the first three repeated batch runs. Hence it can be concluded that the biocatalyst proved to be stable and maintained a

**TABLE 2. Results of Repeated Batch Runs with Nonimmobilized Biomass: A 3-Fold and B 9-Fold Repeated<sup>a</sup>**

repeated run	$c_0$ , $\text{mg dm}^{-3}$	$c_{\text{DCM}}$ , $\text{mg dm}^{-3}$	$R_0^c$ , $\mu\text{g (min mg P)}^{-1}$	$v_0^c$ , $\mu\text{g (min mg P)}^{-1}$	$t_{0.9}$ , min exp	$t_{0.9}$ , min calc
A2	6.5	254	94	88	50	52
A3		257	86	88	58	52
B3	7.9	729	82	68	34	31
B4		701	58	62	28	35
B5		677	54	54	38	30
B6 <sup>b</sup>		807	50	60	27	29
B7		709	46	57	31	34
B8		677	54	58	35	34
B9		624	66	53	40	37

<sup>a</sup>  $R_0$  = rate of initial Hg accumulation in gas traps,  $v_0$  = initial  $\text{Hg}^{2+}$  consumption rate calculated from kinetic law eq 10, and  $t_{0.9}$  = reaction time for 90% conversion. <sup>b</sup> B6 was started after resting overnight. <sup>c</sup>  $R_0$  and  $v_0$  are referred to as a mass of protein by assuming  $c_p = 0.5c_{\text{DCM}}$ .  $R_0$  and  $v_0$  can be converted in  $\mu\text{g dm}^{-3} \text{s}^{-1}$  by multiplying with  $0.5c_{\text{DCM}}/60$ .

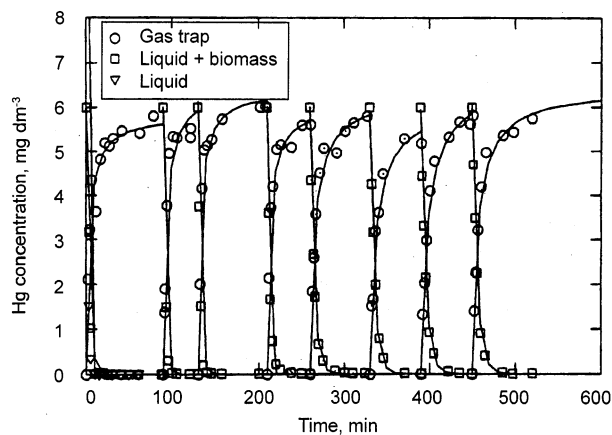


**FIGURE 7. Repeated batch runs of mercury transformation by immobilized *Ps. putida* KT2442::mer-73. Conditions given in Table 3.**

constant activity. In this regard it should be noticed that the mercury adsorbed is always less than 0.1% of the biomass. Such a low loading is also less than 1/10 of the equilibrium value and negligible if compared to the maximum loading  $Q_{\text{max}}$  reported in 3.2.

Batch runs with immobilized biomass are shown in Figure 7. Negligible  $\text{Hg}^{2+}$  adsorption on the immobilized biomass is found, and the residual Hg concentrations in the supernatant liquid are remarkably lower than for runs with free biomass (Figure 6). In particular, no accumulation of Hg is observed. The findings shown in Figure 7 reveal a more stable, robust, and active behavior than found for free biomass. Obviously, immobilization in alginate helps to reduce drastically the Hg adsorption and thus prevents catalyst deactivation.

Mercury biotransformation with *Ps. putida*KT2442::mer73 was studied in continuous operation in the TPFB. The microbes were immobilized in alginate beads with a diameter of 0.9 mm. To decrease the mercury concentration down to the wastewater discharge value of  $50 \mu\text{g dm}^{-3}$  two TPFBs in series were applied. The biomass concentrations in the reactors were 524 and 439  $\text{mg dry biomass per dm}^{-3}$ , respectively. Mercury outlet concentrations for a flow rate of  $1.2 \text{ dm}^3 \text{ h}^{-1}$  were given in Figure 8. The inlet concentration given in the upper part of the graph for the time period indicated varied between 5 and 10  $\text{mg dm}^{-3}$ . The outlet concentration of the first TPFB showed large fluctuations at the beginning but approached an approximately steady-state value of about  $120 \mu\text{g dm}^{-3}$  after a 30-h operation. In the

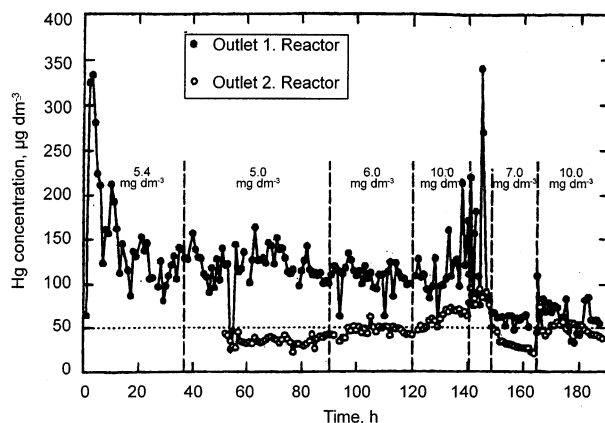


**FIGURE 8. Continuous operation of two TPFB reactors in series – Hg outlet concentration for various inlet concentrations. Flow rate =  $1.2 \text{ dm}^3 \text{ h}^{-1}$  ( $\eta_1 = 0.833 \text{ h}$ ), between  $t = 140$  and  $148 \text{ h}$  the flow rate was increased to  $2.4 \text{ dm}^3 \text{ h}^{-1}$ .**

second reactor a reduction to  $50 \mu\text{g dm}^{-3}$  was achieved. However, the outlet concentration increased when the inlet value was raised to  $10 \text{ mg dm}^{-3}$  for first time. After 140-h operation the flow rate was doubled ( $2.4 \text{ dm}^3 \text{ h}^{-1}$ ) which again temporarily increased the outlet concentrations of both reactors. After reducing the throughput back to  $1.2 \text{ dm}^3 \text{ h}^{-1}$  the reactors rapidly returned to an improved performance. Even the first reactor showed a stable operation for  $10 \text{ mg dm}^{-3}$  at the inlet and reduced the Hg concentration close to the discharge value ( $50 \mu\text{g dm}^{-3}$ ). The mercury removal during the seventh and eighth day of operation is over 99%. The Hg balances over the steady-state operation periods, i.e., the Hg recovers in the reaction medium and in the gas-phase traps were fulfilled by 96–102%.

## 5. Discussion

In the batch runs with nonimmobilized microbes (Figure 6) transport resistances (liquid/solid mass transfer and diffusion) for  $\text{Hg}^{2+}$  can be neglected. Therefore, these runs are appropriate to receive information about the rate of the removal of the produced elemental mercury from the reaction locus. To this end, the Hg accumulation rate  $R_0$  in the gas traps can be used as the gas velocity always applied is high ( $4.9 \text{ cm s}^{-1}$  corresponding to  $246 \text{ cm}^3 \text{ s}^{-1}$ ) and the oxidation of  $\text{Hg}^0$  by  $\text{KMnO}_4/\text{H}_2\text{SO}_4$  in the traps is in the instantaneous regime (12). The initial Hg accumulation rate  $R_0$  is determined for the first 10 minutes after starting the batch runs. On the other hand, the rate of ionic mercury consumption can be calculated from the kinetic expression, eq 10. An average value of the initial  $\text{Hg}^{2+}$  consumption rate  $v_0$  was obtained by estimating from the experiments a mean concentration of  $\text{Hg}^{2+}$  in the TPFB over the first 10 minutes. In addition, the reliability of the rate law, eq 10, particularly in the inhibitory branch, and the exclusion of mass transfer limitations in the runs with free microbes can be checked by integration of eq 10 giving

$$t = \frac{1}{v_{\text{max}}} [K_s \ln(c_0/c_1) + (c_0 - c_1) + (c_0^3 - c_1^3)/3K_1^2] \quad (12)$$

Table 2 summarizes calculated results for 3-fold (Figure 6,A) and 9-fold repeated fed batch runs. Not considered are the first (and second) runs. The rate  $R_0$  and  $v_0$  show reasonable agreement. Also the reaction times for 90% conversion ( $c = 0.1c_0$ ) calculated from eq 12 agree well with the experimental data. This especially confirms the applicability of the kinetic expression to the investigations in the TPFB (with nonimmobilized microbes). The finding that  $R_0$  and  $v_0$  do not differ significantly leads to the important conclusion that removal

of elemental mercury from the TPFB, i.e., gas/liquid mass transfer of  $\text{Hg}^0$  does not effect the overall rate, hence

$$R_0 \leq k_L a \Delta C_{\text{Hg}}^0 \quad (13)$$

With the experimental  $k_L a$  ( $0.022 \text{ s}^{-1}$ ) the driving concentration difference for  $\text{Hg}^0$  transport over the gas/liquid interphase can be estimated

$$R_0/k_L a \leq \Delta c_{\text{Hg}}^0 > c^0 \quad (14)$$

and is found to be larger than the physical solubility of  $\text{Hg}^0$  in water ( $c^0$ ) obtained from eq 2. Therefore, one has to assume that either the liquid phase is supersaturated with  $\text{Hg}^0$  or the fast production rate of  $\text{Hg}^0$  from  $\text{Hg}^{2+}$  by the microbial reaction may lead to formation of  $\text{Hg}^0$  nuclei being quickly volatilized. As the analytical method used did not distinguish between  $\text{Hg}^{2+}$  and  $\text{Hg}^0$ , a discrimination among possibly differing gas/liquid mass transfer mechanisms is therefore not possible. However, the experimental results unambiguously demonstrate that the overall performance of the TPFB is not influenced by  $\text{Hg}^0$  removal even for the case of free microbes with higher effective  $\text{Hg}^{2+}$  conversion rates than the immobilized ones.

Surprisingly when analyzing the batch runs with immobilized microbes (Figure 7) a behavior seemingly similar to the results with a nonimmobilized biocatalyst is found, i.e., the measured overall initial rates ( $R_0$ ) do not differ much from the calculated initial rates  $v_0$  though one would expect significant hindrances by effective diffusion within the immobilized biocatalyst. This observation is understood after analyzing the continuous runs which are easier to interpret due to their steady-state character. The finding  $R_0 \approx v_0$  for the immobilized biocatalyst in the repeated batch runs also indicates that diffusion of generated  $\text{Hg}^0$  in the immobilizee must be fast and does not limit the overall performance as was assumed when introducing Figure 2 and discussing the possibly relevant transport limitations.

For the continuous steady-state runs with the two TPFBs in the series shown in Figure 8 the subsequent analysis is only done for the first reactor. Here the concentration of biomass is  $524 \text{ mg DBM dm}^{-3}$  immobilized in 2000 alginate beads with an average  $d_p$  of 0.9 mm. Transport of  $\text{Hg}^{2+}$  from the bulk liquid ( $c_l$ ) to the surface of the immobilized biocatalyst ( $c_s$ ) is given by (see eq 6)

$$R_{\text{LS}} = k_S a_S (c_l - c_s) \quad (15)$$

$k_S a_S$  is estimated from the experimental data as  $0.0114 \text{ s}^{-1}$ . As the liquid phase of the TPFB is fully mixed and the experimentally obtained mercury concentrations ( $c_l$ ) are low ( $c_l \ll 1 \text{ mg dm}^{-3}$ ) eq 11 can be applied, i.e., the biotransformation takes place in the first-order branch of the kinetic law with  $k = (v_{\text{max}}/K_s) = 0.0373 \text{ s}^{-1}$ . Then, the rate of  $\text{Hg}^{2+}$  conversion  $R_{\text{RD}}$  averaged over the biocatalyst particle follows from

$$R_{\text{RD}} = k \int_0^{d_p/2} c(r) dr \quad (16)$$

Applying reaction-diffusion theory (17, 21) and introducing the effectiveness factor  $\eta$  the average rate can be calculated from

$$R_{\text{RD}} = k \eta c_s \quad (17)$$

TABLE 3. Evaluation of Continuous Runs (in First TPFB)<sup>a</sup>

$c_{l0}$ $\text{mg dm}^{-3}$	$c_l$ $\text{mg dm}^{-3}$	$R_{\text{Exp}}$	$R_{\text{Theor}}$	$R_{\text{RD}}$ ( $\eta = 1$ )
5.4	0.130	1.76	0.40	4.85
5	0.118	1.63	0.38	4.40
6	0.107	1.96	0.35	4.00
10	0.114	3.30	0.37	4.25
7	0.062	2.31	0.20	2.31
10	0.063	3.31	0.20	2.34

<sup>a</sup> Comparison of experimental and theoretically expected mercury transformation rates  $R$  on the basis of different assumptions ( $R$  in  $\mu\text{g dm}^{-3} \text{ s}^{-1}$ ).

with

$$\eta = \left( \frac{D_{\text{eff}}}{d_p^2 k} \right)^{1/2} = 0.12 \quad (18)$$

where  $D_{\text{eff}} = 4.5 \times 10^{-6} \text{ cm}^2 \text{ s}^{-1}$  is estimated from the experimental results with the nonresistant strain (3.3.2). At steady state the rates  $R_{\text{LS}}$  and  $R_{\text{RD}}$  are equal and by combining eqs 15 and 17 with elimination of  $c_s$  the theoretically expected overall rate is given by

$$R_{\text{Theor}} = \frac{c_l}{\frac{1}{k_S a_S} + \frac{1}{k \eta}} \quad (19)$$

By assuming the measured mercury concentration corresponds only to ionic mercury the experimental overall rate follows from

$$R_{\text{Exp}} = D(c_{l0} - c_l) \quad (20)$$

with  $D = F/V = 1.2 \text{ h}^{-1} = 3.33 \times 10^{-4} \text{ s}^{-1}$ . In Table 3 the rates are compiled, and it is clearly discerned that  $R_{\text{Exp}}$  and  $R_{\text{Theor}}$  differ largely. The measured rates are higher by a factor of about 5–10. The situation improves little if liquid/solid mass transfer limitations are neglected ( $1/k_S a_S \ll 1/k \eta$ ). Only if limitations by effective diffusion are not accounted for at all and calculating  $R_{\text{RD}}$  from eq 17 by setting  $\eta = 1$  a reasonable agreement with the experimental data is obtained. As the concentration of nonimmobilized microbes was low and negligible ( $\leq 5 \text{ mg DCM dm}^{-3}$ ) even at long times on stream one has to conclude that the demercuration process in the TPFB is entirely governed by the rate of the biotransformation, eqs 10 and 11, respectively. Hence, all mass transfer resistances are negligible though the live catalyst is encapsulated in alginate. Obviously, this is in accordance with the repeated batch runs using an immobilized catalyst whereby an approximate agreement of  $R_0$  and  $v_0$  was found. Hence, the above conclusion is also apparently valid for the instationary batch run where the  $\text{Hg}^{2+}$  transformation to  $\text{Hg}^0$  mainly takes place in the inhibitory branch of the kinetic expression. However, the first-order kinetic behavior as observed in the continuous runs drastically simplifies the design and scale-up of continuous TPFB for demercuration processes.

The reasons for the unexpected findings, namely, negligibility of diffusional resistances and nonapplicability of the conventional theoretical approach, are not clear. Presently, one can only speculate about the behavior and properties of the live biocatalyst. Further studies are required to better understand the dynamic activity pattern of biofilms and encapsulated microbes, particularly, when investigating substrate inhibited biotransformations as frequently found in microbial remediation processes.

The volumetric  $\text{Hg}^{2+}$  transformation capacity (corresponding to space-time-yield STY) for the continuous runs is about  $12 \text{ g Hg m}^{-3} \text{ h}^{-1}$ . Allowing for larger adaption times the STY can undoubtedly be increased by larger flow rates and higher concentrations of immobilized biomass. One can estimate that STYs up to  $30 \text{ g m}^{-3} \text{ h}^{-1}$  appear easily realizable from a conservative point of view. In the fixed bed reactor the STY is in the range of  $10\text{--}20 \text{ g m}^{-3} \text{ h}^{-1}$  but larger values could also be realized (up to  $30 \text{ g m}^{-3} \text{ g}^{-1}$ ) (22, 23). Therefore, it can be concluded that the TPFB delivers comparable results with regard to the overall volume referred biotransformation capacity.

The experimental results with the two TPFB in series shown in Figure 8 also reveal that the second reactor is not required. The first TPFB gives a conversion of about 99%, and the improvement by the second TPFB is only marginal. It is therefore more appropriate to use a filter with an activated carbon to reduce the  $\text{Hg}^{2+}$  concentration to nil or, at least, below the discharge limit of  $50 \mu\text{g dm}^{-3}$ , respectively. In this regard, the TPFB is assumed to be more effective than the fixed bed as the elemental Hg is completely removed via the gas phase as indicated by coherent mercury balances, i.e., 96–102% recovery. Above all, the application of the TPFB requires no regeneration of the biocatalyst in contrast to the fixed bed process. Therefore, one can expect that the TPFB presents an attractive and favorable alternative to the existing technology.

## Nomenclature

$a$	gas/liquid specific interfacial area, $\text{cm}^{-1}$
$a_S$	liquid/solid specific interfacial area, $\text{cm}^{-1}$
$c$	concentration ( $\text{Hg}^{2+}$ or Hg), $\text{mg dm}^{-3}$
$c^0$	solubility of $\text{Hg}^0$ (eq 2), $\mu\text{g dm}^{-3}$
$c_l$	liquid phase concentration of ionic mercury, $\text{mg dm}^{-3}$
$c_l^*$	liquid-phase concentration of $\text{Hg}^0$ in equilibrium with gas phase, eq 3, $\mu\text{g dm}^{-3}$
$d_p$	particle (immobilizate) diameter, mm
$D$	dilution rate, $\text{s}^{-1}$
$D_{\text{eff}}$	effective diffusivity of $\text{Hg}^{2+}$ in immobilizate, $\text{cm}^2 \text{ s}^{-1}$
$H_e$	Henry's constant (eq 3), $\text{Pa dm}^3 \mu\text{g}^{-1}$
$k_L$	liquid side mass transfer coefficient, $\text{cm s}^{-1}$
$k_S$	liquid side mass transfer coefficient at liquid/solid interface, $\text{cm s}^{-1}$
$K_A$	adsorption equilibrium constant of $\text{Hg}^{2+}$ on microorganisms, $\text{dm}^3 \text{ mg}^{-1}$
$K_S$	affinity constant, $\text{mg dm}^{-3}$
$K_I$	inhibition constant, $\text{mg dm}^{-3}$
$p$	pressure, Pa
$Q$	loading of biomass with adsorbed $\text{Hg}^{2+}$ , $\text{mg g}^{-1}$
$R_{\text{Exp}}$	transformation rate measured experimentally (eq 20), $\mu\text{g dm}^{-3} \text{ s}^{-1}$
$R_0$	initial rate calculated from mercury accumulation in gas traps referred to cell protein mass, $\mu\text{g min}^{-1} \text{ mg}^{-1}$

$R_{\text{RD}}$	rate based on simultaneous effective diffusion and reaction (eq 17), $\mu\text{g dm}^{-3} \text{ s}^{-1}$
$R_{\text{Theor}}$	theoretical rate considering liquid/solid mass transfer, effective diffusion, and first-order reaction (eq 19), $\mu\text{g dm}^{-3} \text{ s}^{-1}$
$t$	time, s
$T$	temperature, K
$u_G$	gas velocity, $\text{cm s}^{-1}$
$v$	specific reaction rate of $\text{Hg}^{2+}$ to $\text{Hg}^0$ (eq 10 or 11), $\mu\text{g min}^{-1} \text{ mg}^{-1}$
$v_0$	initial specific reaction rate, $\mu\text{g min}^{-1} \text{ mg}^{-1}$
$\epsilon_p$	volume fraction of particles
$\eta$	effectiveness factor

## Literature Cited

- (1) *Integrated Pollution Prevention and Control: Reference Document of Best Available Techniques in the Chlor-Alkali Manufacturing Industry*; European Commission Report; 2000. <http://eippcb.jrc.es>
- (2) *Mercury Study Report to Congress (Volume I): 1997*; EPA-452/R-97-003; Office of Air Quality Planning and Standards and Office of Research and Development.
- (3) Mason, R. P.; Fitzgerald, W. F.; Morel, F. M. *Geochim. Cosmochim. Acta* **1994**, *58*, 3191.
- (4) Osborn, A. M.; Bruce, K. D.; Strike, P.; Ritchie, D. A. *FEMS Microbiol. Rev.* **1997**, *19*, 239.
- (5) Nies, D. H. *Appl. Microbiol. Biotechnol.* **1999**, *51*, 730.
- (6) von Canstein, H.; Li, Y.; Timmis, K. N.; Deckwer, W.-D.; Wagner-Döbler, I. *Appl. Environ. Microbiol.* **1999**, *65*, 5279.
- (7) Wagner-Döbler, I.; von Canstein, H.; Li, Y.; Timmis, K. N.; Deckwer, W.-D. *Environ. Sci. Technol.* **2000**, *34*, 4628.
- (8) Fan, L.-S. *Gas-Liquid-Solid Fluidization Engineering*; Butterworth: Boston, 1989.
- (9) Nigam, K. D. P.; Schumpe, A. *Three-Phase Sparged Reactors*; Gordon and Breach Publishers: Amsterdam, 1996.
- (10) Horn, J. M.; Brunke, M.; Deckwer, W.-D.; N. Timmis, K. N. *Appl. Environ. Microbiol.* **1993**, *60*, 357.
- (11) Becker, F. U. Dr. Rer. Nat. Dissertation, Technische Universität Braunschweig, Braunschweig, Germany, 1996.
- (12) Zhao, L.; Rochelle, G. T. *AIChE J.* **1996**, *42*, 3559.
- (13) Crank, J. *The Mathematics of Diffusion*, 2nd ed.; Clarendon Press: Oxford, 1975.
- (14) Arve, B. H.; Liapis, A. I. *AIChE J.* **1987**, *33*, 179.
- (15) Westrin, B. A.; Axelson, A. *Biotech. Bioeng.* **1991**, *38*, 439.
- (16) Akita, K.; Yoshida, F. *Ind. Eng. Chem. Proc. Des. Dev.* **1974**, *13*, 84.
- (17) Deckwer, W.-D. *Bubble Column Reactors*; Wiley: Chichester, 1992.
- (18) Philippidis, G. P.; Schottel, J. L.; Hu, W.-S. *Biotech. Bioeng.* **1991**, *37*, 47.
- (19) Yano, T.; Koga, S. *Biotech. Bioeng.* **1969**, *11*, 139.
- (20) *Gmelin's Handbuch der Anorganischen Chemie*, 2nd ed.; Verlag Chemie: Weinheim, 1967; Vol. 34/B2.
- (21) Levenspiel, O. *Chemical Reaction Engineering*; Wiley: New York, 1972.
- (22) von Canstein, H.; Li, Y.; Leonhäuser, J.; Haase, E.; Felske, A.; Deckwer, W.-D.; Wagner-Döbler, I. *Appl. Environ. Microbiol.* **2002**, *68*, 1938.
- (23) Wagner-Döbler, I.; von Canstein, H.; Li, Y.; Leonhäuser, J.; Deckwer, W.-D. *Chem.-Ing.-Techn.* **2002**, *74*, 504.

Received for review April 16, 2003. Revised manuscript received December 12, 2003. Accepted December 15, 2003.

ES0300517